Fabrication of a cell culture scaffold that mimics the composition and structure of bone marrow extracellular matrix

Short title: Fetal bone marrow ECM as a cell culture scaffold

Ayana Yamaguchi[1], Yoshihide Hashimoto[2], Jun Negishi[1,2 *]

[1]Department of Textile Science and Technology, Graduate School of Science and Technology, Shinshu University, Nagano, Japan

[2]Institute of Biomaterials and Bioengineering, Tokyo Medical and Dental University, Tokyo, Japan

Corresponding author:

Jun Negishi, Dr

Mail address: 3-15-1 Tokida, Ueda, Nagano, JP 386-8567

Tel/fax: +81-268-21-5335

E-mail address: jnegishi@shinshu-u.ac.jp

ABSTRACT

Cell culture models that mimic tissue environments are useful for cell and extracellular matrix (ECM) function analysis. Decellularized tissues with tissue-specific ECM are expected to be applied as cell culture scaffolds, however it is often difficult for seeded cells to permeate their structures. In this study, we evaluated the adhesion and proliferation of mouse fibroblasts seeded onto decellularized bone marrow scaffolds that we fabricated from adult and fetal porcine. Decellularized fetal bone marrow displays more cell attachment and faster cell proliferation than decellularized adult bone marrow. Our findings suggest that decellularized fetal bone marrow is useful as a cell culture scaffold with bone marrow ECM and structure.

Keywords: decellularized fetal bone marrow, extracellular matrix, cell culture scaffold

INTRODUCTION

Human and animal tissues are composed of tissue-specific cells and extracellular matrix (ECM), which, once isolated, can be used for tissue and cell function analysis. Simple two-dimensional (2D) cell culture methods are suitable for elucidating the function of single cells and effects of aqueous factors [1], while co-culture allows evaluation of cell-cell interactions [2, 3]. However, because cells attach to the surface of the culture dish in 2D cultures, the lack of three-dimensional (3D) elements that exist *in vivo* causes cells to behave differently *in vitro* than they would *in vivo* [4].

Recently, 3D culture methods that mimic the state of cells *in vivo* have been used. Spheroids reportedly promote cell-cell interactions and gene expression patterns similar to those *in vivo* due to the close proximity of cells to each other [5, 6]. In addition, organoids composed of stem cells, progenitor cells, and ECM have been applied to the liver and kidney, and used to form the main structures of organs [7]. Importantly, although spheroids and organoids have the advantage of cell aggregation, it is difficult to increase their sizes because oxygen and nutrients must be delivered to the centers [8].

Another approach to 3D culture is using scaffolds composed of metals, polymers, and ceramics to replace the support and functional regulation of cells provided by ECM *in vivo* [9-11]. Scaffold materials derived from ECM, such as collagen, have the advantage of being similar to the *in vivo* environment and are being used for 3D culture of various tissues [12, 13]. Although isolated and purified biomolecules can be used to fabricate scaffold materials with various forms (e.g., gels,

sponges, and nonwoven fabrics), it is difficult to reproduce tissue-specific ECM compositions and structures.

The ECM of biological tissues is a complex 3D structure comprising various proteins and polysaccharides that support cell adhesion, proliferation, and differentiation [14]. Furthermore, the structure and components of biological tissue ECM differ depending on the tissue and animal age [15, 16]. Decellularized tissues and organs are ECM structures and components of native tissues and organs without cells [17]. Seeding cells into a decellularized heart can reportedly recover cardiac function, suggesting that decellularized tissues are useful for 3D cell culture [18].

Bone marrow, located in the center of bones between spongy bone, plays a major role in hematopoiesis [19]. Hematopoiesis is actively carried out in fetal bone marrow and although the proportion of fat increases and hematopoietic capacity declines with growth, blood is produced in the bone marrow throughout life [20, 21]. Bone marrow contains nonadherent blood cells such as leukocytes and erythrocytes derived from hematopoietic stem cells (HSCs), and adherent stromal cells derived from mesenchymal stem cells. HSC proliferation and differentiation appear to be regulated by both stromal cells and bone marrow ECM [14, 22]. Accordingly, a culture system consisting of bone marrow ECM and stromal cells is considered important for the elucidation of hematopoietic mechanisms and drug discovery research. A 3D culture system using decellularized bone marrow as a scaffold material was previously been investigated by Nakamura et al., who used decellularized adult porcine bone marrow as a 3D scaffold for mesenchymal stem cells; however, cells were not introduced throughout the scaffold [23].

Cell functions vary with age and fetal-derived cells display higher proliferation and differentiation potentials than adult-derived cells. In has recently become clear that ECM, like cells, differs in composition and function according to age [24]. Several studies reported that fetal ECM is more conductive to support cell function and tissue formation *in vitro* than adult ECM [25, 26]. Therefore, in this study, we compared differences between fetal porcine decellularized bone marrow and adult porcine bone marrow as a scaffold to mimic the ECM of bone marrow. Mouse fibroblasts (L929), a widely used model cell line, were seeded into scaffolds. The adhesion and proliferation rates of seeded cells were evaluated to investigate the suitability of decellularized bone marrow as a scaffold for 3D cell culture of bone marrow.

MATERIALS AND METHODS

Adult and fetal bone marrow preparation Adult porcine ribs were purchased from Tokyo Shibaura Zouki (Tokyo, Japan) and sliced into approximately 5-mm sections using a bone-cutting knife (Hanchen). Adult bone marrow (ABM) was hollowed out using a punch (φ = 8 mm). Fetal porcine tissue was purchased from a local slaughterhouse. Approximately 5 mm of fetal bone marrow (FBM) was harvested from the top of the femur using a saw and punch (φ = 4 mm).

Decellularization To prepare decellularized adult bone marrow (DABM) and decellularized fetal bone marrow (DFBM), a decellularization treatment was performed according to a previous study [27]. Briefly, ABM and FBM were placed into a polyethylene bag filled with 1× phosphate-buffered saline (PBS; Nacalai Tesque, Kyoto, Japan) that was heat sealed. Next, each bag was pressurized at 1000 MPa for 10 min at 30℃ using a cold isostatic pressurization machine (Dr. Chef; Kobe Steel, Kobe, Japan). To remove cell debris, tissues were first washed with DNase (0.2 mg/mL) (Roche Diagnostics, Tokyo, Japan) in EBM™-2 Medium (Lonza, Walkersville, MD, USA) for 7 d at 37℃. Subsequently, samples were washed with 80% ethanol in saline for 3 d at 37℃. Finally, samples were washed with PBS supplemented with 1% penicillin-streptomycin (PS, Nacalai Tesque) for at least 2 d at 37℃. After washing, tissues were frozen and freeze dried for approximately 72 h using a freeze-drying machine (Alpha 2-4 LSC; CHRIST, Osterode am Harz, Germany).

Cell seeding Mouse fibroblasts (L929) were used as a model cell for scaffold seeding. A suspension of L929 cells was prepared at 2.0×10^6 cells/mL in Dulbecco's Modified Eagle Medium

(DMEM) (Nacalai Tesque) supplemented with 10% fetal bovine serum (FBS) and 1% PS. DABM and DFBM were immersed in the suspension for 10 min.

The cell suspension introduction rate was calculated using Formula 1 with the dry weight (Wd) before cell introduction and wet weight (Ww) after cell seeding. Cell-seeded DABM and DFBM scaffolds were placed in 48-well cell culture plates filled with DMEM supplemented with 10% FBS and 1% PS, and incubated at 37℃ and 5% CO_2 for 5 d. The medium was changed after 1 d and 3 d.

$$\text{Cell suspension introduction rate}\ (\%) = \frac{\mathrm{Ww}-\mathrm{Wd}}{\mathrm{Wd}} \times 100 \ldots (1)$$

Hematoxylin and eosin (HE) staining ABM, FBM, DABM, and DFBM were fixed with a 4% paraformaldehyde (PFA) solution in PBS for 24 h (FUJIFILM Wako Pure Chemical, Osaka, Japan). Samples were dehydrated stepwise by immersion in 70%, 80%, and 90% ethanol for 2 h, respectively, and then 100% ethanol overnight. Samples were then rehydrated by 90%, 80%, and 70% ethanol and decalcified with decalcifying solution B (FUJIFILM Wako Pure Chemical) for 1–2 w with shaking and medium changes every 2 d. After stepwise dehydration, samples were immersed in xylene (FUJIFILM Wako Pure Chemical) for 6 h and embedded in paraffin. Embedded tissues were sliced into 4-μm-thick sections using a microtome (RM2255; Leica, Wetzlar, Germany), and stained with Mayer hematoxylin (Muto Pure Chemicals, Tokyo, Japan) and eosin (Sakura Fintek Japan, Tokyo, Japan). HE-stained sections were observed using a microscope (TSFB-APH; Nikon, Tokyo, Japan).

DNA quantification DNA quantification was performed to evaluate cell removal and cell numbers after seeding of DABM/DFBM. Samples were solubilized using 500 μL of lysis buffer (50

mM Tris-HCl, 100 mM NaCl, 20 mM ethylenediaminetetraacetic acid, 1% sodium dodecyl sulfate, 79% deionized water) and 50 μL of proteinase K (Takara Bio, Shiga, Japan) for 3 d at 55℃. Cells were sonicated by applying ultrasonic waves for 5 min using an ultrasonic cleaning machine. DNA was purified by phenol/chloroform/isoamyl alcohol (25:24:1) (Nippon Gene, Tokyo, Japan) extraction and ethanol precipitation. Purified DNA was dried and dissolved with 500 μL of TE buffer (Nippon Gene). The amount of DNA in each sample was calculated using a Quant-iT™ PicoGreen™ dsDNA Assay Kit (Thermo Fisher Scientific, Waltham, MA, USA).

Scanning electron microscopy (SEM) DABM and DFBM with and without cell seeding were fixed with a 4% PFA solution in PBS for 24 h. Subsequently, scaffolds were dehydrated stepwise by immersion in 70%, 80%, 90%, and 100% ethanol for 2 h. Next, scaffolds were immersed twice in t-butyl alcohol (FUJIFILM Wako Pure Chemical) for 2 h and frozen at −80℃. After freezing, scaffolds were dried under vacuum. Surfaces and cross sections of scaffolds were observed by SEM (JSM-6010LA; JEOL, Tokyo, Japan).

Sodium dodecyl sulfate polyacrylamide gel electrophoresis (SDS-PAGE) Total proteins were extracted from DABM and DFBM using a Total Protein Extraction (TPE™) Kit (Takara Bio). Samples were diluted 1:1 with 2× Laemmli Sample Buffer (Bio-Rad Laboratories, Hercules, CA, USA), heated at 90℃ for 5 min, and then analyzed by electrophoresis at 300 V using an XV Pantera Gel MP (DRC, Tokyo, Japan). After electrophoresis, each gel was washed three times with deionized water for 5 min and stained with CBB Stain One (Nacalai Tesque) for 1 h.

DAPI staining Cell-seeded DABM and DFBM were fixed with a solution of 4% PFA in PBS for 24 h. Scaffolds were then immersed in 30% sucrose and stored at 4℃ for 24 h. Next, samples were embedded in SCEM Cryo-Embedding Medium (Section-Lab, Hiroshima, Japan). Embedded tissues were sliced into 4-μm-thick sections using a cryostat (CM 1950, Leica). After the cryosections were dried, they were mounted using DAPI-Fluoromount-G® (Cosmo Bio, Tokyo, Japan) and observed using a confocal laser-scanning microscope (Olympus, Tokyo, Japan).

Statistical analysis All data are expressed as mean ± standard deviation. Statistical significance was evaluated with a *t*-test. A value of $p < 0.05$ is considered significant.

RESULTS

Preparation of decellularized bone marrow HE staining and DNA quantification were used (Fig. 1) to evaluate the removal of cells from ABM and FBM. There were numerous hematoxylin-stained nuclei in ABM and FBM; however, DABM and DFBM had few stained nuclei. DABM had circular voids with an average diameter of approximately 50 μm between trabecular bones, while DFBM had no circular voids and prominent eosin staining of the ECM (Fig. 1A–D). Amounts of DNA in DABM and DFBM were significantly less than in ABM/FBM ($p<0.01$, Fig. 1E).

Structures and components analysis of decellularized bone marrow SEM observation and SDS-PAGE analysis were performed to compare structures and components of DABM and DFBM (Fig. 2). As observed in the photographs, DABM was overall pale yellow while DFBM was white (Fig. 2A and D). In SEM images, both DABM and DFBM had porous structures. DABM voids were approximately 100–400 μm in diameter and unstructured substances occurred between the trabecular bones (Fig. 2B and C). DFBM had thinner trabecular bone than DABM and voids that were long and narrow (Fig. 2E and F). Two bands around 150 kDa confirmed the identities of DABM and DFBM. A smear band at 10 kDa or less was also observed for DABM, while bands around 75 kDa and 10~15 kDa were also observed for DFBM (Fig. 2G).

Cell seeding in DABM and DFBM Introduction rates of L929 cell suspension into DABM and DFBM indicate that the rate for DFBM was significantly greater than for DABM ($p<0.01$, Fig. 3). To evaluate the proliferation of L929 cells seeded on DABM and DFBM, DNA on the scaffolds was measured after 1 d and 5 d of incubation. L929-seeded DABM did not support cell proliferation

from Day 1 to Day 5; in contrast, L929-seeded DFBM supported cell proliferation from Day 1 to Day 5 ($p<0.01$, Fig. 4).

SEM observations and DAPI staining were performed to evaluate the adhesion and distribution of cells in L929-seeded DABM and DFBM. As observed in SEM images, L929 spheres were slightly attached to the surface of DABM (Fig. 5A–D). In contrast, L929 spheres were attached to the surface and center of DFBM after 1 d of cell seeding and stretched L929 cells were observed after 5 d; indeed, the DFBM surface was covered with numerous cells (Fig. 5E–H).

As observed in DAPI staining images, no cells were observed in DABM after 1 d or 5 d of cell culture (Fig. 6A–D, S-Fig. 1). In contrast, many cells were observed on the surface and in the center of DFBM after 1 d and 5 d, and numbers of cells increased during this time (Fig. 6E and F).

DISCUSSION

In this study, decellularized bone marrow was prepared from adult and fetal porcine tissue to serve as scaffolds that mimic bone marrow ECM. As shown by HE staining, cell numbers decreased after decellularization. In addition, circular voids with an average diameter of approximately 50 μm were observed between trabecular bones in DABM but not DFBM (Fig. 1). Numbers of adipocytes increase with growing postnatal bone marrow and DABM voids display traces of the removed adipocytes. Similar voids with lipid droplets were observed in DABM in a previous study [27]. After the defatting treatment with isopropanol, DABM was confirmed to weigh significantly less than ABM; in contrast, DFBM was similar to FBM, indicating that it had less initial fat (S-Fig. 2). Amounts of residual DNA in both DABM and DFBM were less than 50 ng/mg dry weight [28].

Therefore, cells were successfully removed from both adult and fetal porcine bone marrow tissues. Notably, the DNA content in native FBM was greater than in ABM, suggesting a higher ratio of cells to ECM in FBM. These results may indicate that HSCs in FBM actively proliferate and differentiate, unlike HSCs in ABM that are mostly quiescent [29].

To compare structures and components of DABM and DFBM, SEM observation and SDS-PAGE were performed (Fig. 2). As SEM observations show, thicker trabeculae and larger pores were observed in DABM compared with DFBM. The ECM of ABM is denser than that of FBM ECM because animals produce ECM as they grow [30, 31]. Accordingly, unstructured substances in voids that were barely observed in DFBM were observed in DABM. These substances were reduced after the defatting treatment and not observed in DFBM (S-Fig. 3), indicating that they were likely lipids. As shown in our SDS-PAGE analysis, two bands around 150 kDa confirmed the presence of DABM and DFBM. Collagen type I is an abundant protein in bone marrow. The molecular weights of collagen type I α1 and α2 chains is about 100~150 kDa, therefore the two bands around 150 kDa were assumed to indicate collagen type I α1 and α2 chains [32]. Moreover, a smear band of DABM at 10 kDa or less is not observed for DFBM, suggesting these are lipophilic proteins. Bands of DFBM around 75 kDa and 15 kDa are assumed to indicate bone sialoprotein and bone morphogenetic protein, which are related bone formation [33, 34]. These results indicate that both DABM and DFBM have ECM structure and components.

To clarify the applicability of decellularized bone marrow as a cell culture scaffold, cell seeding was performed. The cell suspension introduction rate of DFBM was significantly greater than

DABM (Fig. 3). DABM contains hydrophobic fats that may inhibit permeation of the cell suspension; alternatively, the cell suspension was able to permeate into DFBM because it contained fewer fats. DNA quantification and SEM observations after cell seeding indicate that the DNA contents of DABM did not increase and only a few cells were observed on the surface of the scaffold (Figs. 4, 5). Because the lipids in DABM inhibited permeation of the cell suspension, cells did not reach the interior. In addition, numbers of adherent cells on DABM were low because cells are less likely to adhere to hydrophobic surfaces [35]. The presence of cells within DABM was not confirmed by DAPI staining; as a result, it was assumed that cell proliferation did not occur (Fig. 6). In contrast, DFBM supported cell attachment and proliferation, and cells were distributed throughout the scaffold. SEM images after cell seeding indicate that the L929 cells that attached to DABM were spherical, whereas most cells that attached to DFBM stretched (especially on Day 5). This result illustrates that the microenvironment of DFBM was suitable for cell attachment and proliferation. Moreover, L929 cells were distributed both on the surface and in the center of DFBM, as observed in DAPI staining images. DFBM is low in lipids, easily permeated by culture medium, and has large pores; therefore, it is presumed that nutrients and oxygen are supplied inside the scaffold. A previous study reported difficulties introducing cells into DABM [23]. However, improvements in cell suspension uptake and cell adhesion to defatted DABM suggest that lipids affect cell penetration and adhesion (S-Figs. 4, 5) [27, 36]. Because the scaffold structure and components affect cell adhesion, proliferation, and differentiation, differences in DABM and DFBM may affect bone marrow cell proliferation and differentiation [37-39].

This study reveals that the ECM structure and components of DABM and DFBM are partially different, and their differences affected adhesion and proliferation of L929 cells in scaffolds. Lipids in DABM were found to interfere with cell permeabilization, while DFBM promoted cell adherence and proliferation. Importantly, because cells readily dispersed throughout DFBM, it may be useful as a 3D-culture substrate. Furthermore, DFBM may be useful as a scaffold to mimic bone marrow ECM. In future research, we plan to establish an *in vitro* model that reproduces the environment regulating hematopoietic function by seeding DFBM with bone marrow stromal cells.

ACKNOWLEDGMENTS

We thank Ashleigh Cooper, Ph.D., from Edanz for editing a draft of this manuscript. This work is supported by JSPS KAKENHI Grant Number 20K20198.

REFERNCES

[1] Piacibello, W., Sanavio, F., Severino, A., Dane, A., Gammaitoni, L., Fagioli, F., Perissinotto, E., Cavalloni, G., Kollet, O., Lapidot, T., and Aglietta, M. (1999). Engraftment in nonobese diabetic severe combined immunodeficient mice of human CD34+ cord blood cells after ex vivo expansion: evidence for the amplification and self-renewal of repopulating stem cells. *Blood, The Journal of the American Society of Hematology*, *93*(11), 3736-3749.

[2] Dexter, T. M., Allen, T. D., and Lajtha, L. G. (1977). Conditions controlling the proliferation of haemopoietic stem cells in vitro. *Journal of cellular physiology*, *91*(3), 335-344.

[3] Jing, D., Fonseca, A. V., Alakel, N., Fierro, F. A., Muller, K., Bornhauser, M., Ehninger, G., Corbeil, D., and Ordemann, R. (2010). Hematopoietic stem cells in co-culture with mesenchymal stromal cells-modeling the niche compartments in vitro. *haematologica*, *95*(4), 542.

[4] Tan, J., Liu, T., Hou, L., Meng, W., Wang, Y., Zhi, W., and Deng, L. (2010). Maintenance and expansion of hematopoietic stem/progenitor cells in biomimetic osteoblast niche. *Cytotechnology*, *62*, 439-448.

[5] Abu-Absi, S. F., Friend, J. R., Hansen, L. K., and Hu, W. S. (2002). Structural polarity and functional bile canaliculi in rat hepatocyte spheroids. *Experimental cell research*, *274*(1), 56-67.

[6] Kelm, J. M., Djonov, V., Ittner, L. M., Fluri, D., Born, W., Hoerstrup, S. P., and Fussenegger, M. (2006). Design of custom-shaped vascularized tissues using microtissue spheroids as minimal building units. *Tissue engineering*, *12*(8), 2151-2160.

[7] Clevers, H. (2016). Modeling development and disease with organoids. *Cell*, *165*(7), 1586-1597.

[8] Gilazieva, Z., Ponomarev, A., Rutland, C., Rizvanov, A., and Solovyeva, V. (2020). Promising applications of tumor spheroids and organoids for personalized medicine. *Cancers*, *12*(10), 2727.

[9] Wang, X., Xu, S., Zhou, S., Xu, W., Leary, M., Choong, P., Qian, M., Brandt, M., and Xie, Y. M. (2016). Topological design and additive manufacturing of porous metals for bone scaffolds and orthopaedic implants: A review. *Biomaterials*, *83*, 127-141.

[10] Liu, X., and Ma, P. X. (2004). Polymeric scaffolds for bone tissue engineering. *Annals of biomedical engineering*, *32*, 477-486.

[11] Bourgine, P. E., Klein, T., Paczulla, A. M., Shimizu, T., Kunz, L., Kokkaliaris, K. D., Coutu, D. L., Lengerke, C., Skoda, R., Schroeder, T., and Martin, I. (2018). In vitro biomimetic engineering of a human hematopoietic niche with functional properties. *Proceedings of the National Academy of Sciences*, *115*(25), E5688-E5695.

[12] Dong, C., and Lv, Y. (2016). Application of collagen scaffold in tissue engineering: recent advances and new perspectives. *Polymers*, *8*(2), 42.

[13] Leisten, I., Kramann, R., Ferreira, M. S. V., Bovi, M., Neuss, S., Ziegler, P., Wagner, W., Knüchel, R., and Schneider, R. K. (2012). 3D co-culture of hematopoietic stem and progenitor cells and mesenchymal stem cells in collagen scaffolds as a model of the hematopoietic niche. *Biomaterials*, *33*(6), 1736-1747.

[14] Lee-Thedieck, C., Schertl, P., and Klein, G. (2022). The extracellular matrix of hematopoietic stem cell niches. *Advanced Drug Delivery Reviews*, *181*, 114069.

[15] Badylak, S. F., Freytes, D. O., and Gilbert, T. W. (2009). Extracellular matrix as a biological scaffold material: Structure and function. *Acta biomaterialia*, *5*(1), 1-13.

[16] Sicari, B. M., Johnson, S. A., Siu, B. F., Crapo, P. M., Daly, K. A., Jiang, H., Medberry, C. J., Tottey, S., Turner, N. J., and Badylak, S. F. (2012). The effect of source animal age upon the in vivo remodeling characteristics of an extracellular matrix scaffold. *Biomaterials*, 33(22), 5524-5533.

[17] Zhang, X., Chen, X., Hong, H., Hu, R., Liu, J., and Liu, C. (2022). Decellularized extracellular matrix scaffolds: Recent trends and emerging strategies in tissue engineering. *Bioactive materials*, 10, 15-31.

[18] Ott, H. C., Matthiesen, T. S., Goh, S. K., Black, L. D., Kren, S. M., Netoff, T. I., and Taylor, D. A. (2008). Perfusion-decellularized matrix: using nature's platform to engineer a bioartificial heart. *Nature medicine*, 14(2), 213-221.

[19] Morrison, S. J., and Scadden, D. T. (2014). The bone marrow niche for hematopoietic stem cells. *Nature*, *505*(7483), 327-334.

[20] Gao, X., Xu, C., Asada, N., and Frenette, P. S. (2018). The hematopoietic stem cell niche: from embryo to adult. *Development*, *145*(2), dev139691.

[21] Veldhuis-Vlug, A. G., and Rosen, C. J. (2018). Clinical implications of bone marrow adiposity. *Journal of internal medicine*, *283*(2), 121-139.

[22] Anthony, B. A., and Link, D. C. (2014). Regulation of hematopoietic stem cells by bone marrow stromal cells. *Trends in immunology*, *35*(1), 32-37.

[23] Nakamura, N., Saito, K., Kimura, T., and Kishida, A. (2020). Recellularization of decellularized cancellous bone scaffolds using low-temperature cell seeding. *Tissue and Cell*, 66, 101385.

[24] Acun, A., Oganesyan, R., Uygun, K., Yeh, H., Yarmush, M. L., and Uygun, B. E. (2021). Liver donor age affects hepatocyte function through age-dependent changes in decellularized liver matrix. *Biomaterials*, *270*, 120689.

[25] Silva, A. C., Rodrigues, S. C., Caldeira, J., Nunes, A. M., Sampaio-Pinto, V., Resende, T. P., Oliveira, M. J., Barbosa, M. A., Thorsteinsdóttir, S., Nascimento, D. S., and Pinto-do-Ó, P. (2016). Three-dimensional scaffolds of fetal decellularized hearts exhibit enhanced potential to support cardiac cells in comparison to the adult. *Biomaterials*, *104*, 52-64

[26] Sood, D., Chwalek, K., Stuntz, E., Pouli, D., Du, C., Tang-Schomer, M., Georgakoudi, I., Black, L. D. III, and Kaplan, D. L. (2016). Fetal brain extracellular matrix boosts neuronal network formation in 3D bioengineered model of cortical brain tissue. *ACS biomaterials science & engineering*, *2*(1), 131-140.

[27] Hashimoto, Y., Funamoto, S., Kimura, T., Nam, K., Fujisato, T., and Kishida, A. (2011). The effect of decellularized bone/bone marrow produced by high-hydrostatic pressurization on the osteogenic differentiation of mesenchymal stem cells. *Biomaterials*, 32(29), 7060-7067.

[28] Crapo, P. M., Gilbert, T. W., and Badylak, S. F. (2011). An overview of tissue and whole organ decellularization processes. *Biomaterials*, 32(12), 3233-3243.

[29] Mikkola, H. K., and Orkin, S. H. (2006). The journey of developing hematopoietic stem cells.

[30] Bonnans, C., Chou, J., and Werb, Z. (2014). Remodelling the extracellular matrix in development and disease. *Nature reviews Molecular cell biology*, *15*(12), 786-801.

[31] Daley, W. P., Peters, S. B., and Larsen, M. (2008). Extracellular matrix dynamics in development and regenerative medicine. *Journal of cell science*, *121*(3), 255-264.

[32] Zhu, L., Xie, Y., Wen, B., Ye, M., Liu, Y., Imam, K. M. S. U., Cai, H., Zhang, C., Wang, F., and Xin, F. (2020). Porcine bone collagen peptides promote osteoblast proliferation and differentiation by activating the PI3K/Akt signaling pathway. *Journal of Functional Foods*, *64*, 103697.

[33] Sodek, K. L., Tupy, J. H., Sodek, J., and Grynpas, M. D. (2000). Relationships between bone protein and mineral in developing porcine long bone and calvaria. *Bone*, *26*(2), 189-198.

[34] Rahmati, M., Khan, A. H., Razavi, S., Khorramizadeh, M. R., Rasaee, M. J., and Sadroddiny, E. (2016). Cloning and expression of human bone morphogenetic protein-2 gene in Leishmania tarentolae. *Biocatalysis and Agricultural Biotechnology*, *5*, 199-203.

[35] Tamada, Y., and Ikada, Y. (1993). Cell adhesion to plasma-treated polymer surfaces. *Polymer*, *34*(10), 2208-2212.

[36] Ranella, A., Barberoglou, M., Bakogianni, S., Fotakis, C., and Stratakis, E. (2010). Tuning cell adhesion by controlling the roughness and wettability of 3D micro/nano silicon structures. *Acta biomaterialia*, 6(7), 2711-2720.

[37] Bacakova, L., Filova, E., Parizek, M., Ruml, T., and Svorcik, V. (2011). Modulation of cell adhesion, proliferation and differentiation on materials designed for body implants. *Biotechnology advances*, 29(6), 739-767.

[38] Gupte, M. J., Swanson, W. B., Hu, J., Jin, X., Ma, H., Zhang, Z., Liu, Z., Feng, K., Feng, G., Xiao, G., Hatch, N., Mishina, Y., and Ma, P. X. (2018). Pore size directs bone marrow stromal cell fate and tissue regeneration in nanofibrous macroporous scaffolds by mediating vascularization. *Acta biomaterialia*, *82*, 1-11.

[39] Karageorgiou, V., and Kaplan, D. (2005). Porosity of 3D biomaterial scaffolds and osteogenesis. *Biomaterials*, *26*(27), 5474-5491.

FIGURES

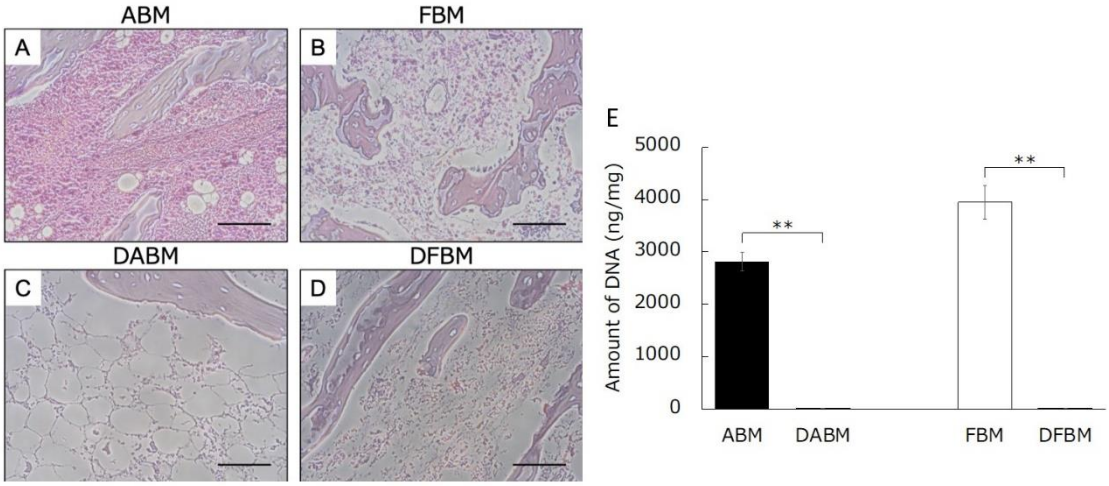

Fig. 1. HE staining images of native and decellularized adult and fetal porcine bone marrow (A-D, scale bar=100 μm). (E)Amount of DNA of native and decellularized adult and fetal porcine bone marrow (n=3, *p < 0.05, **p < 0.01).

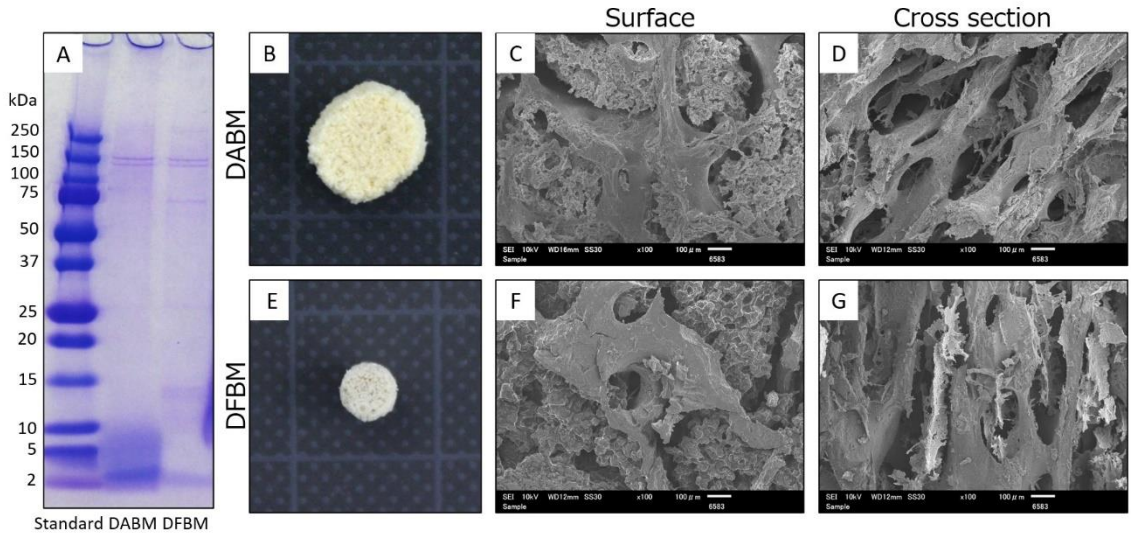

Fig. 2. SDS-PAGE analysis (A) and Photos and SEM images of DABM (B, C, D) and DFBM (E, F, G). (One side of grid is 10 mm (A, D). (scale bar=100 μm, C, D, F, G).

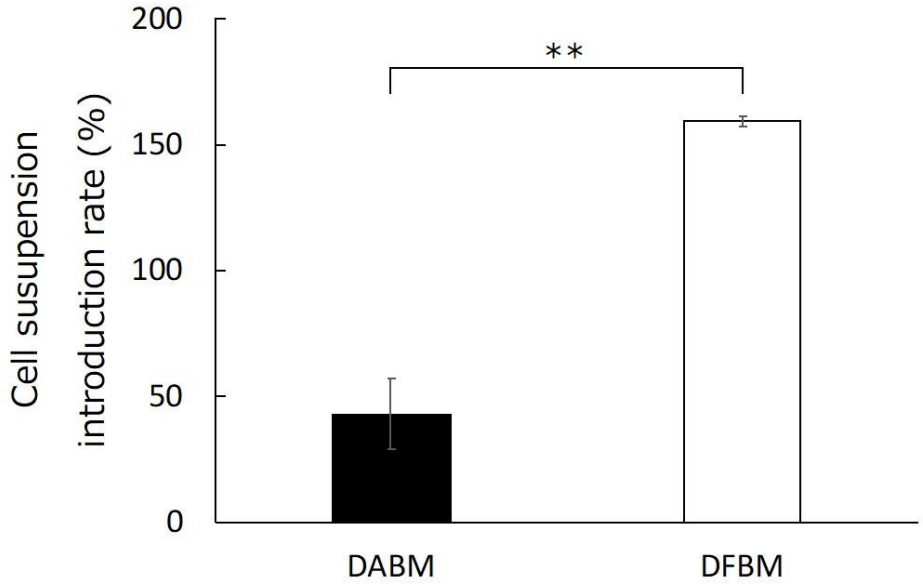

Fig. 3. Cell suspension introduction rate of DABM/DFBM (n=3, **p < 0.01).

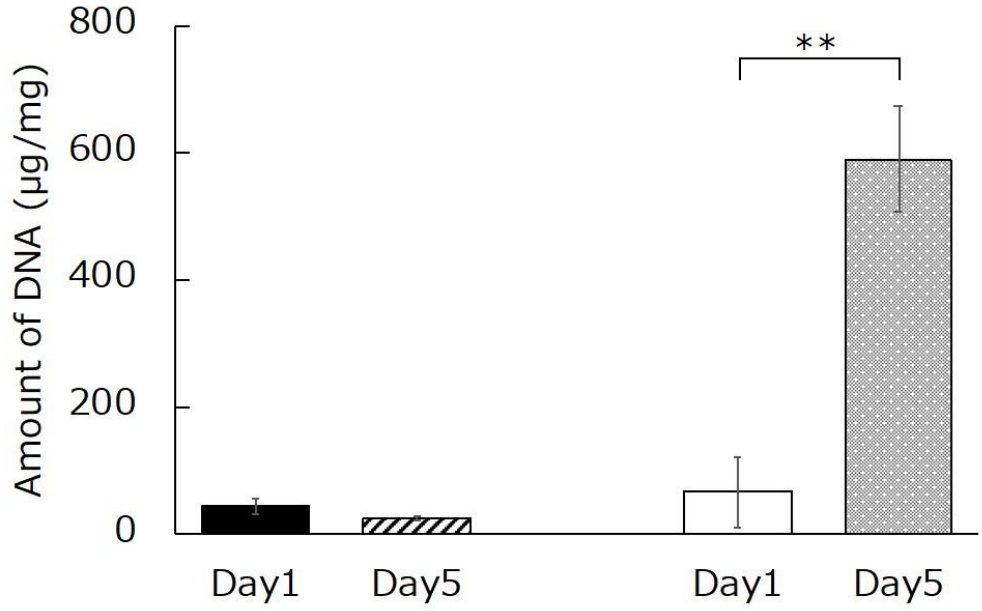

Fig. 4. Amount of DNA of L929 seeded DABM/DFBM after 1 day and 5 days of cell seeding (n=3, *p < 0.05, **p < 0.01). Scaffold is indicated no cell introduction treated DABM/DFBM.

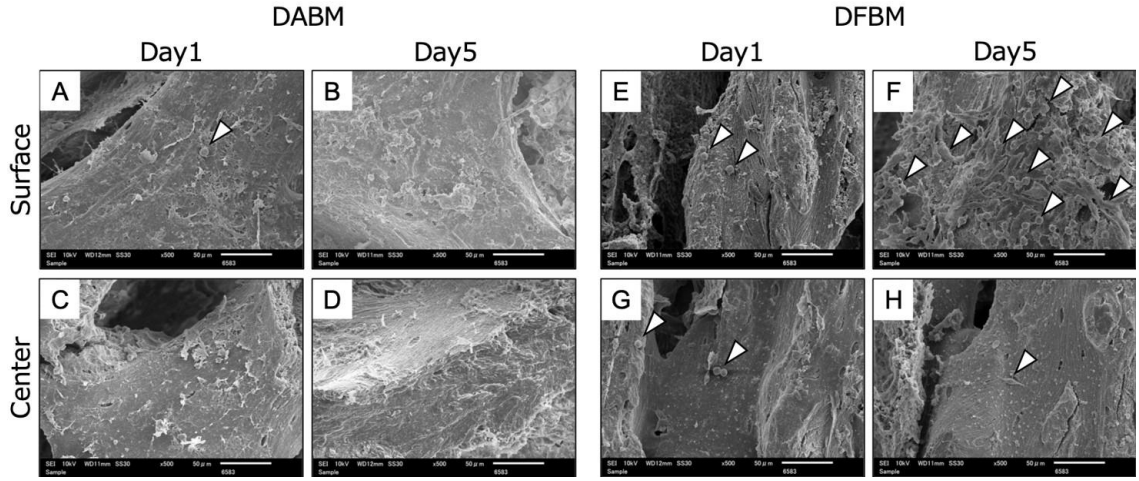

Fig. 5. SEM images of cell attachment on surface and center of L929 seeded DABM/DFBM after 1 day and 5 days of cell seeding (scale bar= 50 μm). Arrow head is L929.

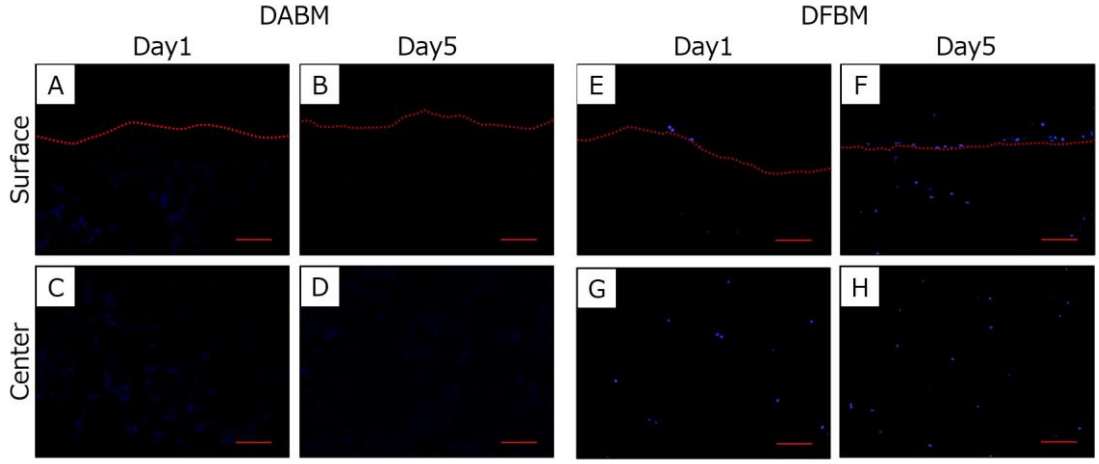

Fig. 6. DAPI staining images of cell distribution in surface and center of L929 seeded DABM/DFBM after 1 day and 5 days of cell seeding (scale bar= 100 μm). Dotted lines are surface of DABM/DFBM.

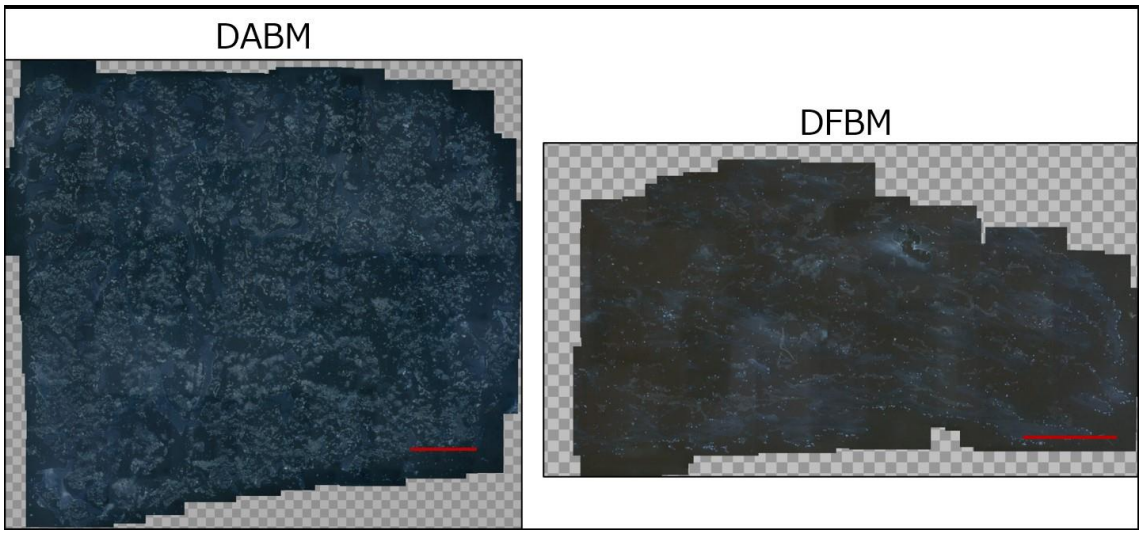

Fig. S1. DAPI staining images of cell distribution in overall scaffolds of L929 seeded DABM/DFBM after 5 days of cell seeding (scale bar=1 mm).

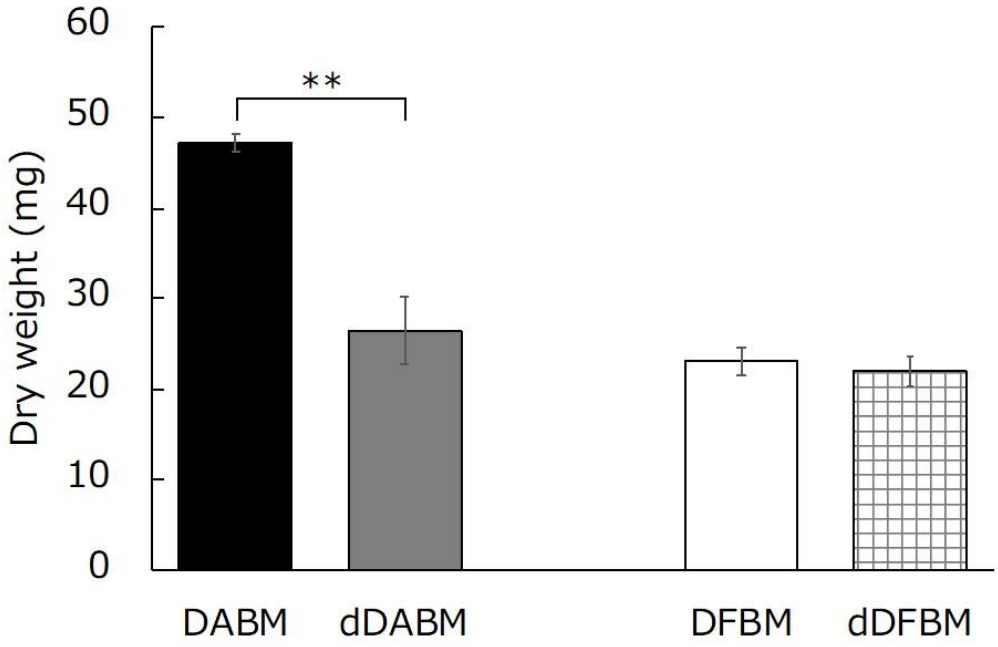

Fig. S2. Dry weight of DABM/DFBM and defatted DABM/DFBM (dDABM/dDFBM) (n=3, **p < 0.01).

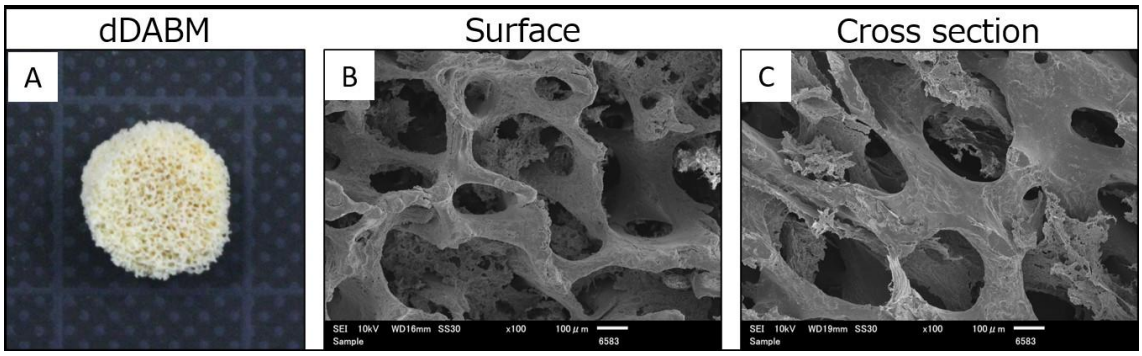

Fig. S3. Photos (A) and SEM images (B, C) of dDABM. One side of grid is 10 mm. (B) surface of dDABM, (C) cross section of dDABM (scale bar=100 μm).

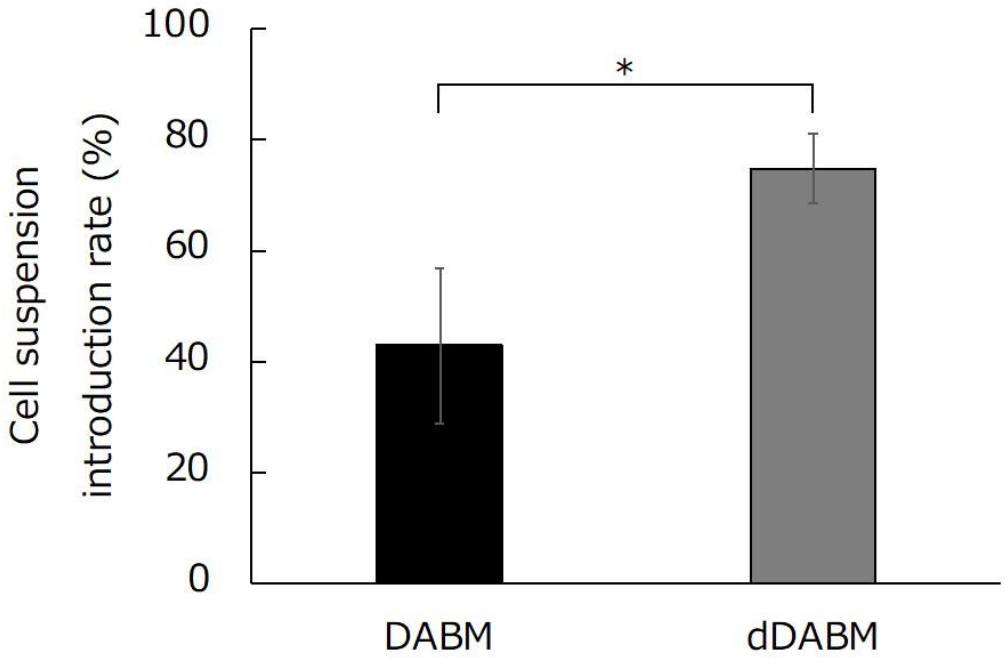

Fig. S4. Cell suspension introduction rate of DABM and dDABM (n=3, *p < 0.05).

1 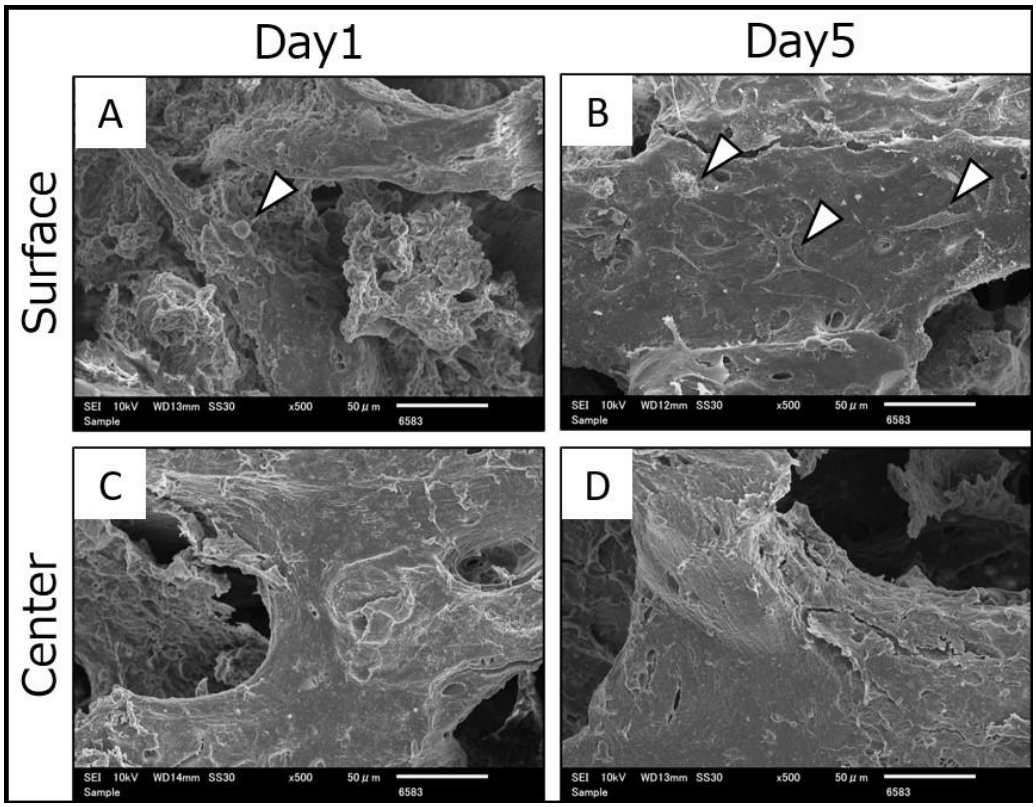

2 Fig. S5. SEM images of cell attachment on surface and center of L929 introduced dDABM after 1

3 day and 5 days of cell seeding (scale bar= 50 μm). Arrow head is L929.